3.1 Introduction

Several studies have been made on electrochemical biosensors during the last four decades [1]. The creation of mediator-based electrochemical sensors has made use of redox mediators. Numerous studies have been done using ferrocene and its derivatives as effective electrocatalysts. Because it is an excellent organometallic one-electron reservoir and one of many redox mediators, ferrocene (Fc) is a popular electroactive molecule [2,3]. Fc-modified surfaces have consistently perfect electrochemical properties and have outstanding electrochemical stability, according to cyclic voltammetry measurement. Pd-modified Fc-based materials offer versatile electrochemical applications due to synergistic effects [4]. The reversible oxidation of air- and water-stable ferrocene (Fc) to Fc^+ makes it an excellent internal standard in electrochemistry. In general, ferrocene's chemical and physical properties and its derivatives can be used in a broad range of applications, including sensing, materials research, and catalysis [5]**.** Under mild potential conditions, the ferrocenium ion (Fc^+) is generated from the basic unit of ferrocene (Fc) via a reversible oxidation process. Due to this characteristic, ferrocene is perfect for usage in supramolecular systems that require straightforward redox chemicals at the surface of the electrode [6].

Ascorbic acid (AA), is a crucial nutrient for people and is found in both the animal and plant worlds, where it plays a vital role in cellular metabolism. It aids in the growth of new cells, the recovery of wounds and burns, and the production of collagen, blood vessels, bones, cartilage, and tendons [7]. Among other things, fruits and vegetables are the primary sources of the water-soluble substance ascorbic acid. It is well-known for its medicinal use, antioxidant impact on foods and beverages, and reductive capabilities. To oxidize ascorbic acid in an aqueous solution, chemically modified electrodes with a variety of active mediators

immobilized at the electrode surfaces were used. On the other hand, an overdose of AA can cause chemical conversion into oxalate, contributing to an increase in the level of oxalate in urine and, in the long run, the development of kidney stones [8].

AA has been detected in biological fluids, food, and pharmaceutical formulations using spectroscopy, chromatography, chemiluminescence, optical sensors, and electrochemical methods. Electrochemical methods receive a lot of interest due to their quick reaction, easy instrumentation, high sensitivity, compactness, *in vivo* detection capabilities, low cost, and ease [9,10]. It has also been shown that the alkyl chain connected to the amine group affects how easily nanoparticles (NPs) disperse in organic and aqueous media. Furthermore, the functional ability of organic amine attached to the alkoxysilane group enables the usage of 3-APTMS for altering nano shape, functional ability, dispersibility, and processability in a single step, which facilitates the synthesis of AuNPs, PdNPs, and Au-Pd [11,12]. The role of EETMS, GPTMS, and 3-aminopropyltrimethoxysilane (3-APTMS) in the synthesis of gold nanoparticles (AuNPs) with regulated nano geometry has been thoroughly investigated. A similar mechanism is found for the conversion of 3-APTMS capped Pd^{2+} ions. The time taken to create noble metal nanoparticles ranges from 2 to 10 min, justifying the use of EETMS, 3-APTMS, GPTMS, formaldehyde, and PVP as the most efficient reagents [13,14].

Pd-Fc/Fcmc activity is recognized by using 3-Aminopropyltrimethoxysilane (3-APTMS) and organic reducing agents such as cyclohexanone/formaldehyde, introducing another effective method for controlling nanoparticle synthesis and catalytic activity. For two fundamental reasons, Fc/Fc^{+} evolved into the redox couple that epitomizes organometallic electrochemistry-1) quick and kinetically straightforward, the ferrocene self-exchange process, and 2) its rate is not affected by the solvent. At the solid electrode, the heterogeneous electron transport is

electrochemically reversible, comparably fast, and not hampered by homogeneous processes [15]. Numerous ferrocene derivatives satisfy the following requirements for ideal redox mediators, including (a) reversibility, (b) regeneration at minimal potentials, (c) low molecular mass, (d), consistency of each form of the redox couple, and (e) insensitivity to pH consistency of each form of the redox couple [2].

Carbon paste electrodes have been one of the most common microporous matrixes for exploring mediated bioelectrochemistry. Two mixtures of hydrophobic and hydrophilic alkoxysilanes, such as 3-glycidyloxypropyl trimethoxysilane (GPTMS); 3-APTMS and 2-(3,4 epoxycyclohexyl) ethyltrimethoxysilane (EETMS), respectively, were used at an inadequate ratio to encapsulate ferrocene and ferrocene monocarboxylic acid (Fcmc). When the Fc and Fcmc was encapsulated within an ormosil film made from palladium linked-GPTMS and 3-APTMS, the reversible electrochemistry was excellent, even more adequate than the exact measurement made in a homogeneous solution. When used in controlled electrochemical sensing, the nano shape thin film was able to speed up the regeneration of redox enzymes [16–18].

The aim of the present work is to investigate the following; (i) the role of Pd nano-geometry on the redox electrochemistry of Fc and Fcmc (ii) to better understand how nanostructured palladium and Fc, Fcmc modified electrodes work towards ascorbic acid determination.

3.2 Experimental

3.2.1 Materials Ferrocene (Fc), ferrocene monocarboxylic acid (Fcmc), graphite powder (particles size < 20 μm), Nujol oil (density 0.838 g/ml), K_2PdCl_4, were obtained from Sigma Aldrich Chemical Co. India. Ascorbic acid, anhydrous disodium hydrogen phosphate (Na_2HPO_4), and Dihydrogen sodium phosphate mono hydrates ($NaH_2PO_4.H_2O$) were obtained

from HiMedia Chemicals, India. 3-Aminopropyltrimethoxysilane(3-APTMS) and 2-(3,4-epoxycyclohexyl) ethyltrimethoxysilane (EETMS) were purchased from TCI India. All chemicals were of analytical grade and were used as received without further purification.

3.2.2 Synthesis of Palladium Nanoparticles (PdNPs)

PdNPs1 The PdNPs1 have been synthesized by the previously reported method [19] which involves mixing of methanolic solution of K_2PdCl_4 (10 mM) 80 µl, Polyvinyl pyrrolidone (PVP 1%) 20 µl and EETMS (10 mM) 20 µl. Stirred the solution on cyclo mixture and kept in the oven for 5-10 min for incubation at 40-50 °C. The brownish-black colloidal solution is obtained and represented as PdNPs1.

PdNPs2 50 µL of 10 mM of K_2PdCl_4 solution in methanol was premixed with 10 µL of methanolic solution of 3-APTMS (0.5 to 5.4 M) stirred for 2 min, followed by the addition of 50 µL formaldehyde. The solution was kept under the microwave oven for incubation for 70 s. The black colloidal solution was obtained [20].

3.3 Measurement and Characterization

Transmission electron microscopy (Tecnai G2 20 TWIN, FEI Electron Optics) was used to analyze the shapes and sizes of palladium nanoparticles. The synthesized PdNPs were confirmed by powder XRD (Rigaku mini flex 600 Japan).

3.3.1 Preparation of Modified Carbon Paste Electrode (CPE)

Palladium nanoparticles (PdNPs1&PdNPs2) were adsorbed on graphite powder as it was obtained. Pd nanoparticle with graphite was made by mixing 100 µl Pd nanoparticle sol with 100 mg graphite powder (particle size 2-20 µm) and ultrasonicated for 30 min. To ensure complete drying, the mixtures were kept at 60 °C overnight. To remove the organic functionality of the Palladium nanoparticles accumulated on graphite were calcined at 500 °C

in an N_2 gas environment. In a grinder, the solid residues (which contained Palladium nanoparticles adsorbed on graphite powder) were mixed entirely with ferrocene and ferrocene monocarboxylic acid (Fcmc). The presence or absence of PdNPs in the active paste led to the production of modified carbon paste electrode (CPE) systems such as CPE/Fc, CPE/Fcmc, CPE/Fc-PdNPs1, CPE/Fcmc-PdNPs1, CPE/Fc-PdNPs2, and CPE/Fcmc-PdNP2. The borosilicate glass capillaries were used to the fabricate the carbon paste electrodes. The well of the glass capillary was filled with a modified carbon paste containing the ingredients shown in **Table 3.1**.

Table 3.1 Composition of the mediator-modified electrodes

System	Fc/Fcmc (w/w%)	PdNPs adsorbed on graphite(w/w%)	Graphite (w/w%)	Nujol oil (w/w%)
Fc/Fcmc	2.0	-	68	30
Fc-PdNPs1/ Fcmc-PdNPs1	2.0	10	58	30
Fc-PdNPs2/ Fcmc-PdNPs2	2.0	10	58	30

3.3.2 Electrochemical Measurement

The electrochemical experiments were recorded using a computer-controlled electrochemical workstation Model CHI 660B TX, USA. Using an experimental set-up where the resistance was gradually compensated for the uncompensated state, each CV was recorded many times. Using a three-electrode cell setup with a working capacity of 3 ml, the measurements were performed. An Ag/AgCl electrode (RE1B, ALS Co. Japan) and a Pt foil electrode are used as reference and counter electrodes. All potentials given below were relative to the Ag/AgCl. The

modified carbon paste electrode was used as a working electrode. Analysis of the effect of sweep rates on peak current was carried out by recording cyclic voltammograms at different scan rates starting at 0.01 Vs^{-1} to 0.5 Vs^{-1}. Ascorbic acid (AA) was detected using cyclic voltammetry (CV), differential pulse voltammetry (DPV), and amperometry i-t curve. The working electrolyte used for the all-electrochemical study was 0.1 M phosphate buffer solution (pH 7.0) having 0.5 M KCl as supporting electrolyte. Freshly prepared AA was used for all experiments, concentration is mentioned wherever is required. All the experiments were performed at ambient temperature and under similar conditions.

3.4 Results and Discussion

3.4.1 Fabrication and Characterization of Pd Nanoparticles

The current study displays the usage of two different sizes of palladium, i.e., PdNPs1 and PdNPs2 to investigate their effects on the oxidation & reduction electrochemistry of Fcmc and Fc. The XRD data is shown in **figure 3.1**, illustrates five unique reflection planes, all of which are allocated to 2θ values according to JCPDS#87-641, 40^{o} (111), 46.47° (200), 68.04° (220), 81.73° (311) and 86.23° (222).

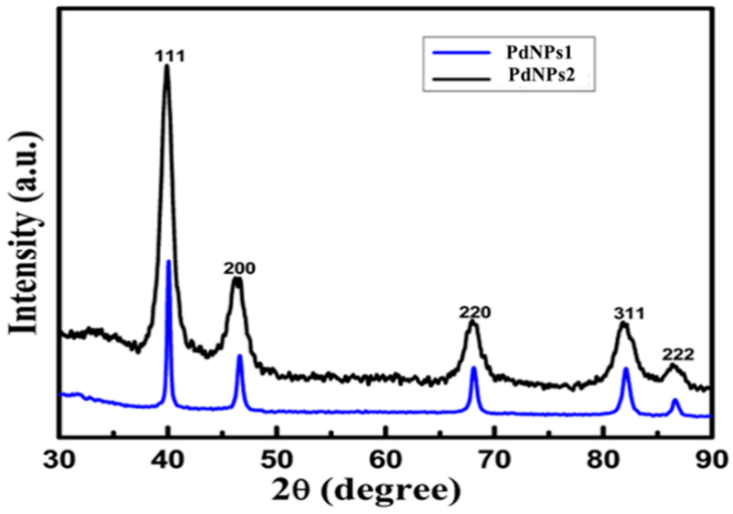

Figure 3.1 XRD pattern of the PdNPs1 & PdNPs2

Figure 3.2(a, d) shows the TEM examination of PdNPs1 and PdNPs2. The PdNPs1 shape look likes agglomerate nanosphere while PdNPs2 are spherical, triangular and cube like structures as clearly seen in the TEM pictures **figure 3.2** (a, d). The average particle size was calculated to be 18 nm ± 2 nm for PdNPs1 and 8 nm ± 2 nm for PdNPs2 and shown in histogram **figure 3.2** (c, f). SAED revealed the crystalline nature of the nanoparticles in **figure 3.2** (b, e).

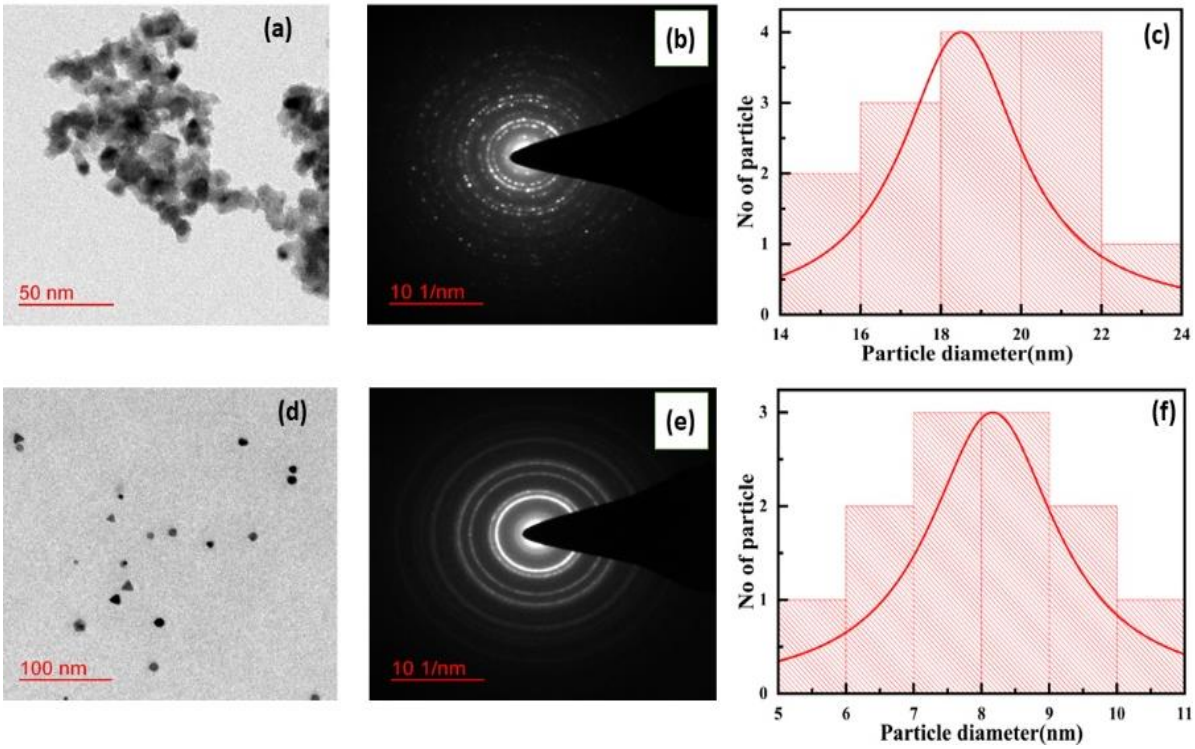

Figure 3.2 TEM images (a, d) along with corresponding SAED patterns (b, e) and histograms (c, f) of the PdNPs1 & PdNPs2, respectively.

3.4.2 The Influence of Pd nanoparticles shape on redox electrochemistry of Ferrocene and Ferrocene carboxylic acid

To study the effects of palladium nanoparticles on Fc and Fcmc redox electrochemistry, these two nanoparticles were used to form Fc-PdNPs1 and Fc-PdNPs2. The findings on the change in redox performance of Fc and Fcmc within the modified carbon paste electrode (CPE) were examined first. The cyclic voltammograms of (a) CPE/Fc, (b) CPE/Fc-PdNPs1, (c) CPE/Fc-

PdNPs2, (d)CPE/Fcmc, (e)CPE/Fcmc-PdNPs1, and (f) CPE/Fcmc-PdNPs2 electrodes at varied scan rates are shown in **figure 3.3**.

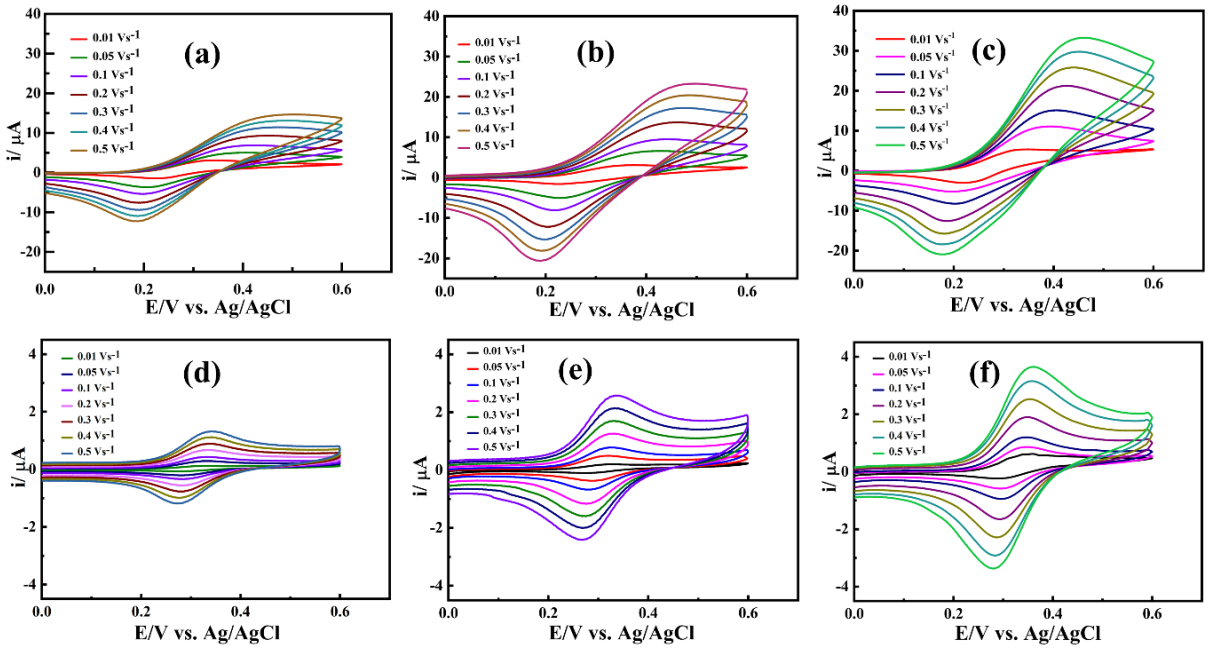

Figure 3.3 Cyclic voltammetry of CPE/Fc (a), CPE/Fc-PdNPs1 (b), CPE/Fc-PdNPs2 (c), CPE/Fcmc (d), CPE/Fcmc-PdNPs1 (e), and CPE/Fcmc-PdNPs2 (f) in 0.1 M phosphate buffer (0.5M KCl, supporting electrolyte) between 0 to 0.6 V vs Ag/AgCl at different scan rates starting at 0.01 Vs^{-1} to 0.5 Vs^{-1}.

The drop in difference between anodic (E_{pa}) and cathodic (E_{pc}) peak potentials is found to be higher with CPE/Fcmc-PdNPs2 electrode which may be due to varied nanogeometry of PdNPs2 as shown in **figure 3.3**. Furthermore, under comparable conditions, both anodic and cathodic peak currents steadily increase, showing a reduction in charge transfer resistance as a function of palladium nano geometry, which is further validated by impedance spectroscopy. Following that, we used cyclic voltammetry and differential pulse voltammetry to investigate the dynamic electrochemistry in the presence and absence of varying concentrations of ascorbic acid, as ascorbic acid is an efficient electroactive species that can be used for both electrochemistry direct and mediated.

The outcomes as proven in **figure 3.4** truly justify significant enhancement in anodic current attributed to the electrochemical transformation of ascorbic acid once more confirming a decrease in charge transfer resistance as a function of palladium nanogeometry.

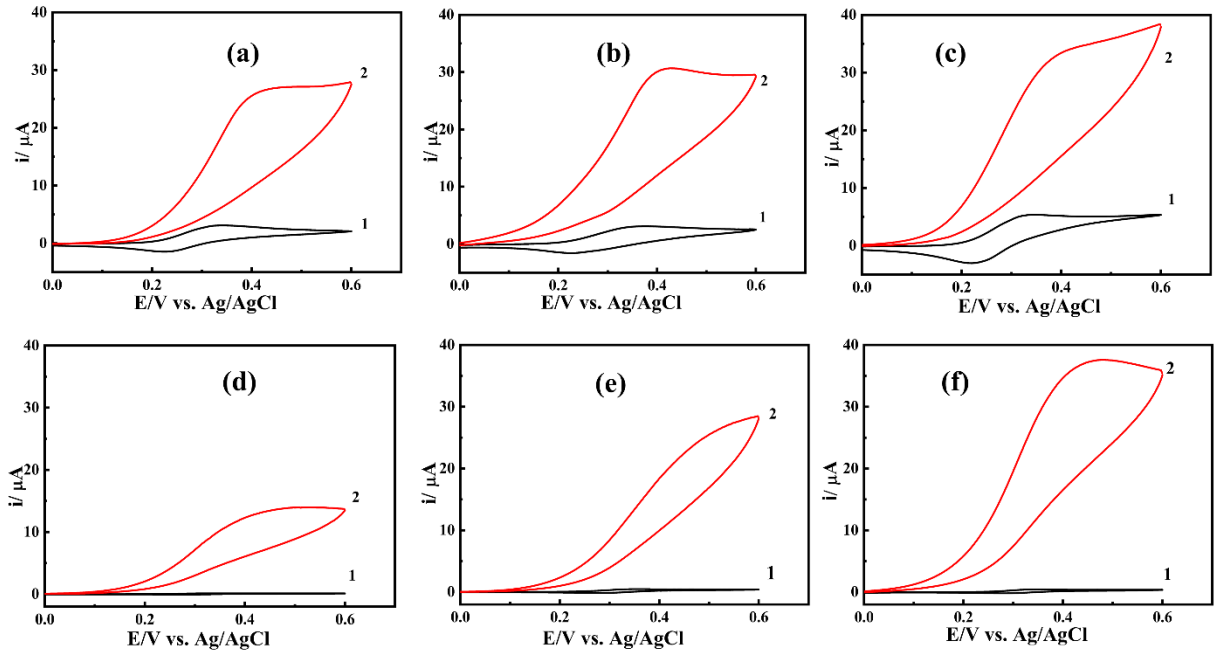

Figure 3.4 Cyclic voltammograms at 10 mV/s before (curve 1) and after (curve 2) addition of ascorbic acid (5 mM) for CPE/Fc (a), CPE/Fc-PdNPs1 (b), CPE/Fc-PdNPs2 (c), CPE/Fcmc (d) CPE/Fcmc-PdNPs1 (e), and CPE/Fcmc-PdNPs2 electrodes, respectively.

An electroanalytical study of modified carbon paste electrodes was performed by amperometric measurement under stirring conditions **figure 3.5** shows the results of amperometric measurements using AA (5 µM to 1.6 mM) in a continuously stirred solution with an operating potential of 0.31V vs Ag/AgCl. **Figure 3.5** shows that CPE/Fcmc-PdNPs2 has higher responses than CPE/Fcmc-PdNPs1, CPE/Fcmc, CPE/Fc, CPE/Fc-PdNPs1 and CPE/Fc-PdNPs2 modified electrode.

As illustrated in **figure 3.5** (a, b) standard curve for AA detection by amperometry was performed. The findings point to a strong linear relationship between amperometric current and AA concentration.

The change in the sensitivity of CPE/Fc, CPE/Fc-PdNPs1, CPE/Fc-PdNPs2, CPE/Fcmc, CPE/Fcmc-PdNPs1 and CPE/Fcmc-PdNPs2 electrodes for AA was observed to be 11.03, 17.42, 23.36, 19.85, 33.02, and 43.96 µA/mM, respectively, confirming the role of palladium and its nano geometry on electroanalysis and further confirmed via amperometric responses recorded at varying running potentials between 0.15 V and 0.4 V vs Ag/AgCl as proven in **figure 3.5.**

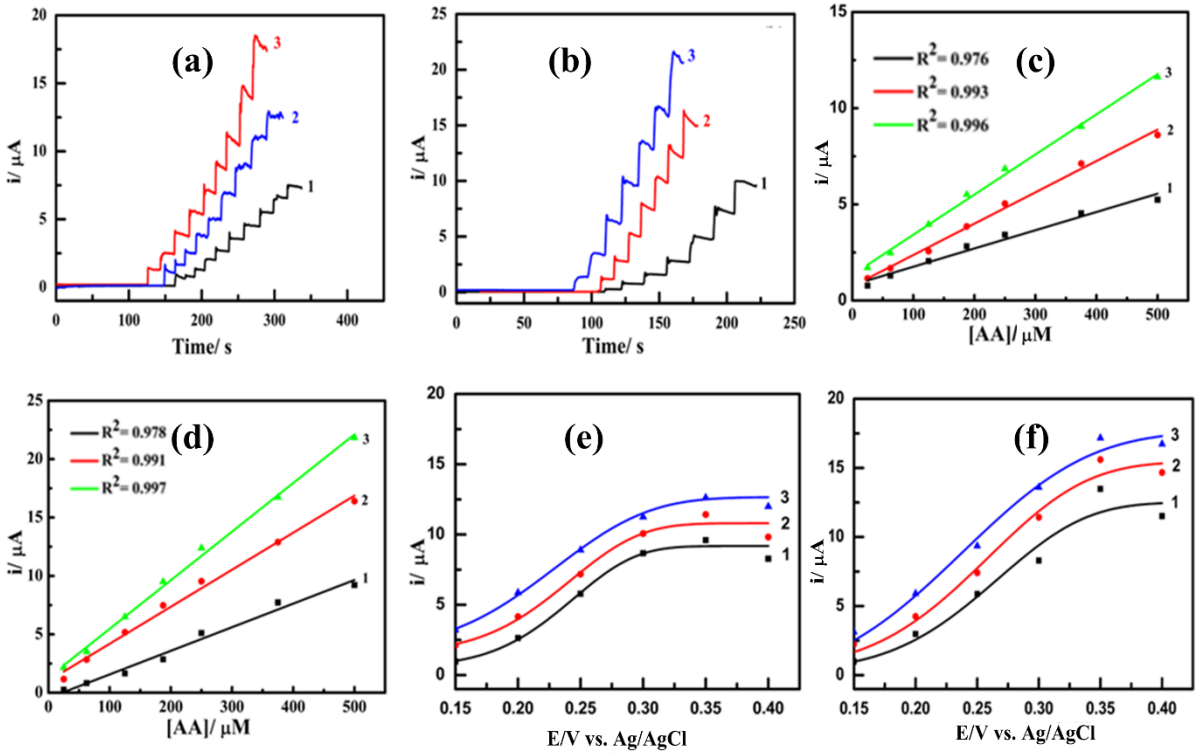

Figure 3.5 Amperometric response of (a) CPE/Fc (1), CPE/Fc-PdNPs1 (2), CPE/Fc-PdNPs2 (3), (b) CPE/Fcmc (1), CPE/Fcmc-PdNPs1 (2), and CPE/Fcmc-PdNPs2 (3) on the addition of varying concentrations of ascorbic acid. Calibration curve (c) CPE/Fc (1), CPE/Fc-PdNPs1 (2), CPE/Fc-PdNPs2 (3), and (d) CPE/Fcmc (1), CPE/Fcmc-PdNPs1 (2), and CPE/Fcmc-PdNPs2 (3), and curve (e, f) were recorded at a different operating potential between 0.15 to 0.4 V vs Ag/AgCl for ascorbic acid determination.

Following that, the impact of palladium and its nanogeometry during electrochemical sensing was examined using differential pulse voltammetry (DPV) of CPE/Fc, CPE/Fc-PdNPs1, CPE/Fc-PdNPs2, CPE/Fcmc, CPE/Fcmc-PdNPs1, and CPE/Fcmc-PdNPs2 electrodes. Figure 3.6(a, b, c, d, e, and f) show differential pulse voltammograms at various ascorbic acid concentrations.

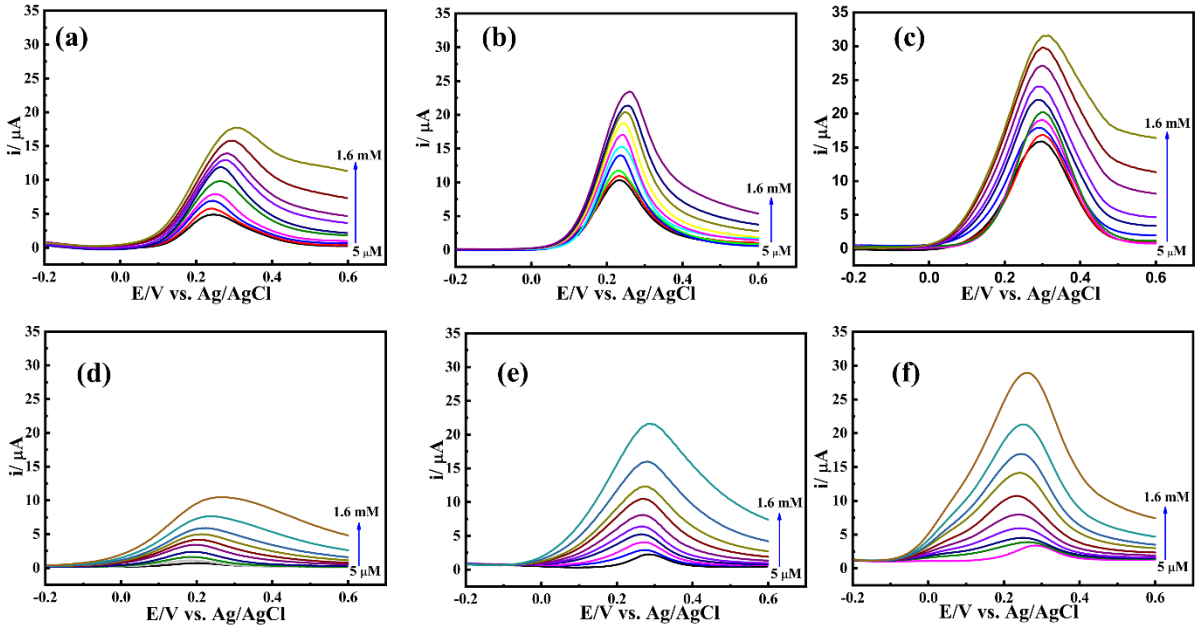

Figure 3.6 Differential pulse voltammetry of CPE/Fc (a), CPE/Fc-PdNPs1 (b), CPE/Fc-PdNPs2 (c), CPE/Fcmc (d) CPE/Fcmc-PdNPs1 (e), and CPE/Fcmc-PdNPs2 (f) in the presence of varying concentrations of ascorbic acid (5 µM to1.6 mM) under similar condition.

Figure 3.7 shows the calibration curves 1,2, and 3, for pulse voltammogram peak currents as a function of ascorbic acid. With a progressive rise in ascorbic acid sensitivity, a linear corelations was found between differential pulse voltammetry current and AA concentration. The sensitivity of AA for CPE/Fc, CPE/Fc-PdNPs1, Fc-PdNPs2, CPE/Fcmc, CPE/Fcmc-PdNPs1 and CPE/Fcmc-PdNPs2 electrodes was found to be 7.45, 9.89, 12.18, 5.91, 12.31 and 16.75 µA/mM, respectively, validating the role of palladium and its nanogeometry.

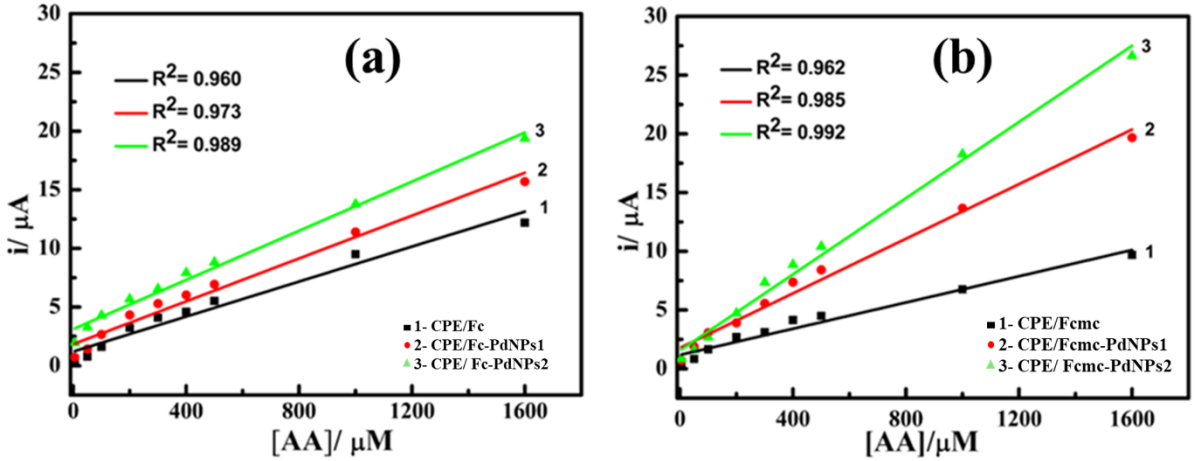

Figure 3.7 The linear relation between differential pulse voltammogram peak currents vs concentration of ascorbic acid (a) Fc and (b) Fcmc modified electrodes system, respectively.

The findings in **figure 3.4** and **figure 3.6** can be investigated further to better understand the impact of palladium and its nanogeometry, as shown in **figure 3.8**, which demonstrates the variation of the current function $i_a/\nu^{1/2}$ as a function of scan rate.

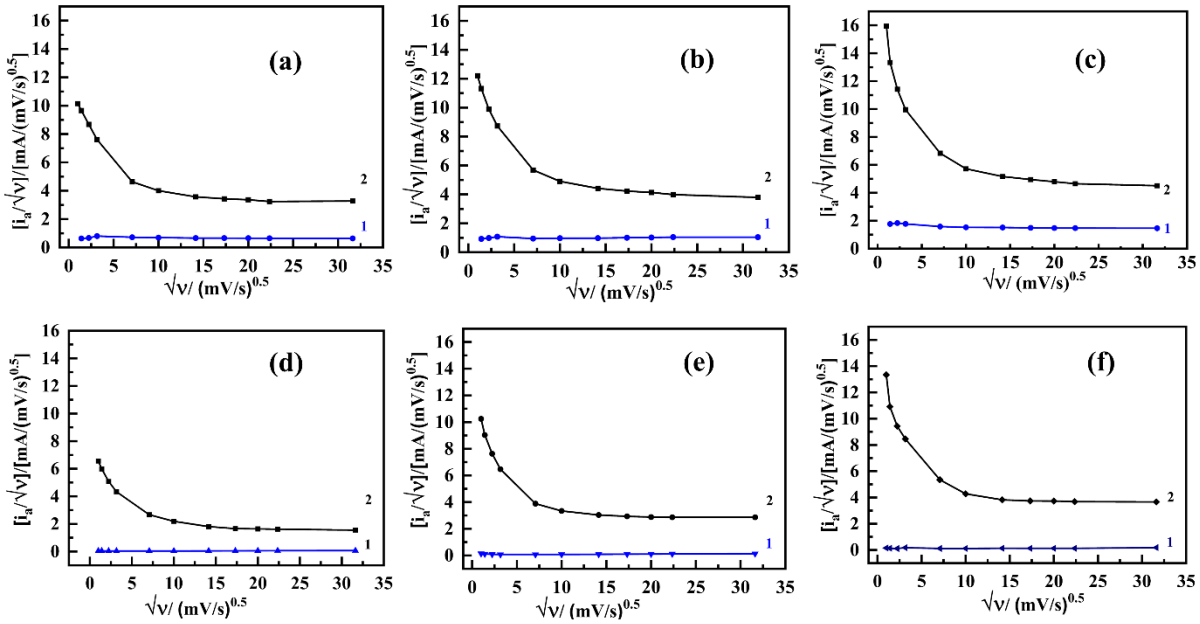

Figure 3.8 The plot of current function vs square root of scan rate of CPE/Fc (a), CPE/Fc-PdNPs1 (b), CPE/Fc-PdNPs2 (c), CPE/Fcmc (d) CPE/Fcmc-PdNPs1 (e), and CPE/Fcmc-PdNPs2 (f).

In the absence of ascorbic acid, the results of the variation of current function on scan rate in all six cases CPE/Fc, CPE/Fc-PdNPs1, CPE/Fc-PdNPs2, CPE/Fcmc, CPE/Fcmc-PdNPs1, and

CPE/Fcmc-PdNPs2 electrodes showed a horizontal straight line, whereas, with ascorbic acid, the current function gradually decreases as scan rate increases and eventually tends to a straight line. The characteristics of the proposed sensor are compared to those of existing sensors reported in the literature for the detection of ascorbic acid in **Table 3.2**.

Table 3.2 Comparison of the modified electrodes with previously reported sensors

Electrode material	Method	Detection limit (µM)	Linear range	Reference
Pt foil	Amperometry	-	0.570-5.680 mM	[21]
ERGO[a]/GCE	DPV	250.0	0.5-2.0 mM	[22]
CuO/rGO	CV	189	0.5-2.0 mM	[23]
Pd-Pt/ rGO	DPV	0.61	40-1200 µM	[24]
MCM41	DPV	10	40-400 µM	[9]
G[b]-30	SWV	17.8	5-1000 µM	[25]
HNGA[c]	DPV	16.7	50-1500 µM	[26]
7-hCNT/MA[d]	SWV	50	200-750 µM	[27]
PANI-TCNQ-Pd[e]	Amperometry		0.05-5mM	[18]
CPE/Fc-PdNPs2 / CPE/Fcmc-PdNPs2	Amperometry	5	10-500 µM	**This work**

[a] Electrochemically reduced graphene oxide. [b] G30-graphene ink. [c] Holy nitrogen-doped graphene aerogel.
[d] Seven-hole carbon nanotube paste multielectrode array. [e] Polyaniline tetracyanoquinodimethane Palladium.

The current response increases in magnitude when ascorbic acid is added, as shown in curve 2 of Figure 3.8. However, this current magnitude diminishes with increasing scan rates. The

higher current response was obtained with the modified electrodes CPE/Fc-PdNPs2, and CPE/Fcmc-PdNPs2 which implying faster charge transfer dynamics as a function of palladium nanogeometry.

3.4.3 Study of Electrochemical Impedance Spectroscopy (EIS)

EIS experiments were also carried out to study the effect of change of nanogeometry on charge transfer characteristics, for CPE/Fc, CPE/Fc-PdNPs1, CPE/Fc-PdNPs2, CPE/Fcmc, CPE/Fcmc-PdNPs1, and CPE/Fcmc-PdNPs2 electrodes in 0.1 M phosphate buffer solution (with 0.5 M KCl) in absence and presence of AA, between 1 Hz and 100 kHz, and 0.31V, and 0.28 V potential were used as shown in **figure 3.9**. Randle's circuit has two halves on a standard Nyquist plot: one is semi-circular, and the other is linear. At a lower frequency, the linear element represents the mass transfer diffusion-restrained process, whereas, at a higher frequency, the diameter of the semicircle represents the charge transfer resistance.

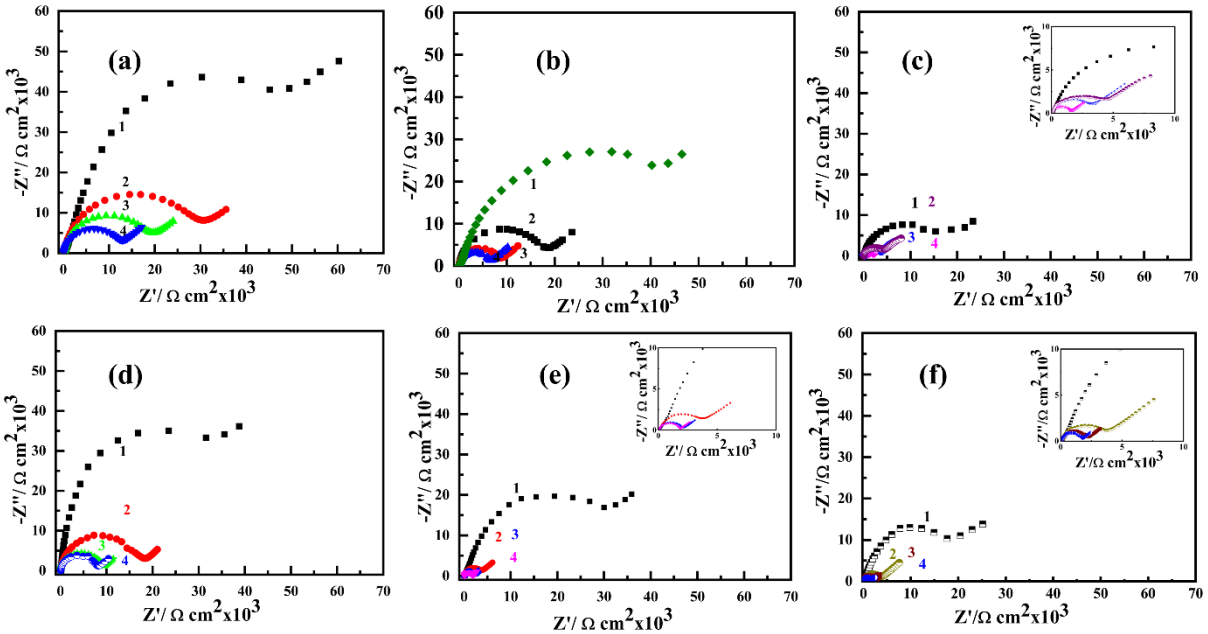

Figure 3.9 Nyquist plot of CPE/Fc (a), CPE/Fc-PdNPs1 (b), CPE/Fc-PdNPs2 (c), CPE/Fcmc (d) CPE/Fcmc-PdNPs1 (e), and CPE/FcmcPdNPs2 (f), with vary concentration of (1) blank, (2) 2.5 mM, (3) 5 mM and (4) 7.5 mM.

The charge transfer resistance (R_{ct}) of the system is represented by the diameter of the circle component inside the Nyquist plot. CPE/Fcmc-PdNPs2 has a lower R_{ct} (1.58 kΩ cm^2) than CPE/Fcmc-PdNPs1(1.87 kΩ cm^2), CPE/Fc-PdNPs2 (1.96 kΩ cm^2), CPE/Fc-PdNPs1 (6.87 kΩ cm^2), CPE/Fcmc (8.34 kΩ cm^2), and CPE/Fc (12.85 kΩ cm^2), indicating that the system CPE/Fcmc-PdNPs2 has the highest charge transfer. In addition, as the concentration of ascorbic acid rises, the diameter of the circle shrinks, and the charge transfer process gradually accelerates. The inset figure is shown for clear visuality.

Table 3.3 shows the calculated charge transfer resistance values for CPE/Fc, CPE/Fc-PdNPs1, CPE/Fc-PdNPs2, CPE/Fcmc, CPE/Fcmc-PdNPs1, and CPE/Fcmc-PdNPs2 electrodes, demonstrating the impact of palladium and its nanostructures on the redox electrochemistry of Fcmc and Fc.

Table 3.3 Table for charge transfer resistance for the modified electrodes

Concentration	Modified Electrodes					
	Fc R_{ct} kΩ cm^2	Fc-Pd NPs1 R_{ct} kΩ cm^2	Fc-Pd NPs2 R_{ct} kΩ cm^2	Fcmc R_{ct} kΩ cm^2	Fcmc-Pd NPs1 R_{ct} kΩ cm^2	Fcmc-Pd NPs2 R_{ct} kΩ cm^2
blank	60	50	30	55	45	15.5
2.5 mM (AA)	35	19.5	5.39	18.5	4.76	4.57
5.0 mM (AA)	21.1	9.8	3.1	9.7	2.34	2.1
7.5 mM (AA)	12.85	6.87	1.96	8.34	1.87	1.58

As a result, the charge transfer resistance of the ferrocene and ferrocene monocarboxylic acid modified electrode is reduced, allowing for faster dynamic electrochemistry.

3.5 Conclusions

The results of the experiments reveal that varying the nanogeometry of Pd nanoparticles aids in improving the sluggish electrochemistry of Fc and Fcmc in ascorbic acid sensing. The goal of this study was to accelerate the dynamic electrochemistry of Fc and Fcmc, which is important in electrochemical sensing, in the presence of palladium with two distinct nanogeometry. As the nanogeometry of PdNPs changes, the electrochemistry of Fc and Fcmc improves. In the presence of palladium, the slow electrochemistry of the Fc and Fcmc modified electrode accelerates, with a progressive increase in peak current as a function of palladium nanogeometry. Even at higher scan rates, the current function as a function of palladium nanostructures tends to be dependent, indicating a potential benefit of palladium and its nanogeometry in redox-mediated electrochemistry. These results show that the Fc-PdNPs1 and Fcmc-PdNPs2 exhibit excellent reproducible and stable electrochemical behavior while detecting ascorbic acid.

3.6 References

[1] M.J. Tierney, H.O.L. Kim, Electrochemical Gas Sensor with Extremely Fast Response Times, *Anal. Chem.*, **65** (1993): 3435–3440. https://doi.org/10.1021/ac00071a017.

[2] N.G. Tsierkezos, U. Ritter, Electrochemical impedance spectroscopy and cyclic voltammetry of ferrocene in acetonitrile/acetone system, *J. Appl. Electrochem.*, **40** (2010): 409–417. https://doi.org/10.1007/s10800-009-0011-3.

[3] N. Changsan, S. Chairam, P. Jarujamrus, M. Amatatongchai, Sensitive electrochemical sensor based on gold nanoparticles assembled ferrocene-functionalised graphene oxide modified glassy carbon electrode for simultaneous determination of dopamine and acetaminophen, *Adv. Nat. Sci.: Nanosci. Nanotechnol.*, **13** (2022): 015012. https://doi.org/10.1088/2043-6262/ac5d44.

[4] P.C. Pandey, B.C. Upadhyay, Role of Palladium in the Redox Electrochemistry of Ferrocene Monocarboxylic Acid Encapsulated Within ORMOSIL Networks, *Molecules*, **10** (2005): 728–739. https://doi.org/10.3390/10060728.

[5] H. Beitollahi, M.A. Khalilzadeh, S. Tajik, M. Safaei, K. Zhang, H.W. Jang, M. Shokouhimehr, Recent Advances in Applications of Voltammetric Sensors Modified with Ferrocene and Its Derivatives, *ACS Omega*, **5** (2020): 2049–2059. https://doi.org/10.1021/acsomega.9b03788.

[6] L. Fernández, H. Carrero, Electrochemical evaluation of ferrocene carboxylic acids confined on surfactant–clay modified glassy carbon electrodes: oxidation of ascorbic acid and uric acid, *Electrochim. Acta*, **50** (2005): 1233–1240. https://doi.org/10.1016/J.electacta.2004.08.016.

[7] G. huang Wu, Y. fang Wu, X. wei Liu, M. cong Rong, X. mei Chen, X. Chen, An electrochemical ascorbic acid sensor based on palladium nanoparticles supported on graphene oxide, *Anal. Chim. Acta*, **745** (2012): 33–37. https://doi.org/10.1016/j.aca.2012.07.034.

[8] S. Qiu, S. Gao, L. Xie, H. Chen, Q. Liu, Z. Lin, B. Qiu, G. Chen, An ultra-sensitive electrochemical sensor for ascorbic acid based on click chemistry, *Analyst*, **136** (2011): 3962–3966. https://doi.org/10.1039/c1an15316a.

[9] D. Sun, Y. Zhang, F. Wang, K. Wu, J. Chen, Y. Zhou, Electrochemical sensor for simultaneous detection of ascorbic acid, uric acid and xanthine based on the surface enhancement effect of mesoporous silica, *Sens. Actuators B: Chem.*, **2** (2009): 641–645. https://doi.org/10.1016/j.snb.2009.07.043.

[10] P.R. Lima, P.R.B. de Miranda, A.B. de Oliveira, M.O.F. Goulart, L.T. Kubota, Modified Carbon Paste Electrode for Kinetic Investigation and Simultaneous Determination of Ascorbic and Uric Acids, *Electroanalysis*, **21** (2009): 2311. https://doi.org/10.1002/elan.200904694.

[11] P.C. Pandey, A.K. Pandey, G. Pandey, Functionalized alkoxysilane mediated controlled synthesis of noble metal nanoparticles dispersible in aqueous and non-aqueous medium, *J. Nanosci. Nanotechnol.*, **14** (2014): 6606–6613. https://doi.org/10.1166/jnn.2014.9378.

[12] P.C. Pandey, R. Singh, A.K. Pandey, Tetrahydrofuran hydroperoxide and 3-aminopropyltrimethoxysilane mediated controlled synthesis of Pd, Pd-Au, Au-Pd nanoparticles: Role of Palladium nanoparticles on the redox electrochemistry of ferrocene monocarboxylic acid, *Electrochim. Acta*, **138** (2014): 163–173. https://doi.org/10.1016/j.electacta.2014.06.101.

[13] P.C. Pandey, R. Singh, Y. Pandey, Controlled synthesis of functional Ag, Ag–Au/Au–Ag nanoparticles and their Prussian blue nanocomposites for bioanalytical applications, *RSC Adv.*, **5** (2015): 49671–49679. https://doi.org/10.1039/c5ra06251a.

[14] P.C. Pandey, M.D. Mitra, S. Shukla, R.J. Narayan, Organotrialkoxysilane-Functionalized Noble Metal Monometallic, Bimetallic, and Trimetallic Nanoparticle Mediated Non-Enzymatic Sensing of Glucose by Resonance Rayleigh Scattering, *Biosensors*, **11** (2021): 122. https://doi.org/10.3390/bios11040122.

[15] L. Fabbrizzi, The ferrocenium/ferrocene couple: a versatile redox switch, *ChemTexts*, **6** (2020): 1–20. https://doi.org/10.1007/s40828-020-00119-6.

[16] J.B. Raoof, R. Ojani, F. Chekin, Electrochemical Analysis of D-Penicillamine Using a Carbon Paste Electrode Modified with Ferrocene Carboxylic Acid, *Electroanalysis*, **19** (2007): 1883–1889. https://doi.org/10.1002/elan.200703947.

[17] P.C. Pandey, S. Upadhyay, N.K. Shukla, S. Sharma, Studies on the electrochemical performance of glucose biosensor based on ferrocene encapsulated ORMOSIL and glucose oxidase modified graphite paste electrode, *Biosens. Bioelectron.*, **18** (2003): 1257–1268. https://doi.org/10.1016/s0956-5663(03)00075-7.

[18] P.C. Pandey, V. Singh, P.C. Pandey, V. Singh, Electrochemical polymerization of aniline over tetracyanoquinodimethane encapsulated ormosil matrix: application in the electrocatalytic oxidation of ascorbic acid and acetylthiocholine, *Analyst*, **136** (2011): 1472. https://doi.org/10.1039/c0an00491j.

[19] P.C. Pandey, S. Shukla, Solvent dependent fabrication of bifunctional nanoparticles and nanostructured thin films by self assembly of organosilanes, *J. Solgel. Sci. Technol.*, **86** (2018): 650–663. https://doi.org/10.1007/s10971-018-4686-y.

[20] Chitra Singh, K. Singh, Prem.C. Pandey, Synthesis and Properties of Organotrialkoxysilane Functionalized Palladium–Cobalt Heterogeneous Catalysts for Oxygen Evolution Reaction, *Russ. J. Electrochem.*, **59** (2023): 604–615. https://doi.org/10.1134/s1023193523080074.

[21] Y.C. Weng, Y.L. Hsiao, Comparison of Pt and Ni foil electrodes for amperometric sensing of ascorbic acid, *J. Electroanal. Chem.*, **651** (2011): 160–165. https://doi.org/10.1016/j.jelechem.2010.11.031.

[22] L. Yang, D. Liu, J. Huang, T. You, Simultaneous determination of dopamine, ascorbic acid and uric acid at electrochemically reduced graphene oxide modified electrode, Sens. Actuators B: Chem., **193** (2014): 166–172. https://doi.org/10.1016/j.snb.2013.11.104.

[23] A. Singh, A. Sharma, A. Ahmed, S. Arya, Highly selective and efficient electrochemical sensing of ascorbic acid via CuO/rGO nanocomposites deposited on conductive fabric, *Appl. Phys. A: Mater. Sci. Process*, **128** (2022): 262. https://doi.org/10.1007/s00339-022-05436-w.

[24] J. Yan, S. Liu, Z. Zhang, G. He, P. Zhou, H. Liang, L. Tian, X. Zhou, H. Jiang, Simultaneous electrochemical detection of ascorbic acid, dopamine and uric acid based on graphene anchored with Pd-Pt nanoparticles, *Colloids Surf. B: Biointerfaces*, **111** (2013): 392–397. https://doi.org/10.1016/j.colsurfb.2013.06.030.

[25] L. Fu, A. Wang, G. Lai, W. Su, F. Malherbe, J. Yu, C. te Lin, A. Yu, Defects regulating of graphene ink for electrochemical determination of ascorbic acid, dopamine and uric acid, *Talanta*, **180** (2018): 248–253. https://doi.org/10.1016/j.talanta.2017.12.058.

[26] S. Feng, L. Yu, M. Yan, J. Ye, J. Huang, X. Yang, Holey nitrogen-doped graphene aerogel for simultaneously electrochemical determination of ascorbic acid, dopamine and uric acid, *Talanta*, **224** (2021): 121851. https://doi.org/10.1016/j.talanta.2020.121851.

[27] Y. Peng, D. Zhang, C. Zhang, Simultaneous voltammetric determination of ascorbic acid and uric acid using a seven-hole carbon nanotube paste multielectrode array, *Anal. Methods*, **6** (2014): 8965–8972. https://doi.org/10.1039/c4ay01029a.